

Vortex reflection at boundaries of Josephson-junction arrays.T. J. Hagenaars^{1,*}, J. E. van Himbergen¹, Jorge V. José², and P. H. E. Tiesinga¹¹*Instituut voor Theoretische Fysica,**Princetonplein 5, Postbus 80006, 3508 TA Utrecht, The Netherlands*²*Department of Physics, Northeastern University,**Boston Massachusetts 02115, USA*

(July 6, 1995)

Abstract

We study the propagation properties of a single vortex in square Josephson-junction arrays (JJA) with free boundaries and subjected to an applied dc current. We model the dynamics of the JJA by the resistively and capacitively shunted junction (RCSJ) equations. For zero Stewart-McCumber parameter β_c we find that the vortex always escapes from the array when it gets to the boundary. For $\beta_c \geq 2.5$ and for low currents we find that the vortex escapes, while for larger currents the vortex is reflected as an antivortex at one edge and the antivortex as a vortex at the other, leading to a stationary vortex oscillatory state and to a non-zero time-averaged voltage. The escape and the reflection of a vortex at the array edges is qualitatively explained in terms of a coarse-grained model of a vortex interacting logarithmically with its image. For $\beta_c \geq 50$ we find that the reflection regime is split up in two disconnected regimes separated by a second vortex escape regime. When considering an explicit vortex-antivortex pair in an array with periodic boundaries, we find a soliton-like non-destructive collision in virtually the same current regimes as where we find reflection of a single vortex at a free boundary; outside these current regimes the pair annihilates. We also discuss the case when the free boundaries are at 45 degrees with respect to the current direction, and thus the angle of incidence of the vortex to the boundaries is 45 degrees. Finally, we study the effect of self-induced magnetic fields (for penetration depths ranging from 10 to 0.3 times the lattice spacing) by taking into account the full-range inductance matrix of the array and find qualitatively equivalent results. We also discuss possible consequences of these results to experimental systems.

PACS numbers: 74.50.+r, 74.60.Ge, 74.60.Jg, 74.70.Mq

I. INTRODUCTION

In recent years the viscous motion of a single vortex in two-dimensional Josephson-junction arrays (JJA) has been studied numerically by several authors [1–7]. In these studies the I-V characteristics were calculated for JJA with periodic boundary conditions perpendicular to the direction of the applied dc current. Apart from the vortex viscosity, the nature of its predicted mass [8–14] has attracted significant interest, also experimentally [15,16]. Van der Zant et al. reported experimental evidence for ballistic motion of vortices in a current-free region in a highly underdamped Josephson-junction array [15].

An interesting aspect of this problem, which is relevant to experiments such as those in [15], but that has not yet been studied systematically, is the influence of boundaries on the vortex motion. Experimentally one may distinguish two types of boundaries (see e.g. Ref. [15]): either the junctions at the edge are connected to a superconducting busbar or they are not (free boundary). The influence of the boundary on a vortex due to the busbar geometry can be described by an image vortex of the same sign, equidistant on the other side of the boundary; in the free boundary case the image of the vortex is of opposite sign. The latter situation is to some extent analogous to that of a soliton in a continuous long Josephson junction (LJJ) [17–19].

The goal of this paper is to study the reflection, transmission and annihilation properties of vortices in JJA with free boundaries. Here, we report simulations of dc biased arrays with free boundaries, in zero applied magnetic field. For every bias current considered we use the same initial phase configuration with one vortex in the middle of the array. We study the dynamical interaction of the vortex with the free boundary as it moves towards it for bias currents above the depinning threshold. The vortex-boundary interaction is equivalent to the effect of an image antivortex at equal distance on the other side of the boundary. A vortex and an antivortex interact logarithmically (at sufficiently large distances), so the same holds for a vortex and a free boundary. The total effective vortex potential is the sum of the interaction potential and the periodic lattice pinning potential. The Lorentz force on the vortex due to the applied bias current corresponds to a tilt of this effective potential. Below we will see this more explicitly when we discuss the coarse-grained model equations for the vortex dynamics.

The outline of this paper is the following. In section II we define the model equations studied in this paper. There we consider the extreme type-II limit (infinite penetration depth) as well as the case of finite penetration depth. We also discuss the coarse-grained vortex equations which are used to analyze the results later in the paper. In section III (a) we present results in the extreme type-II regime and in III (b) the results for finite magnetic penetration depth. In section IV we analyze the results from III (a) in terms of the coarse-grained, phenomenological vortex equations including the interaction of the vortex with the free boundaries. In section V we present results for a vortex moving in diagonal JJA. Section VI contains a summary of our results and some conclusions.

II. MODEL EQUATIONS

In JJA vortices are represented by patterns of eddy current around a plaquette. We consider dc-biased JJA in the classical regime defined by $E_J \gg E_c = e^2/2C$, where E_J is

the Josephson coupling energy and E_c the characteristic charging energy of a junction, e the electron charge, and C the mutual capacitance of the junctions. In this case, and in zero applied magnetic field, the individual junctions in the JJA can be modeled by the resistively and capacitively shunted junction (RCSJ) model [20], defined by the total bond current $i(\mathbf{r}, \mathbf{r}')$ between nearest neighbor sites \mathbf{r} and \mathbf{r}' as

$$i(\mathbf{r}, \mathbf{r}') = \beta_c \ddot{\theta}(\mathbf{r}, \mathbf{r}') + \dot{\theta}(\mathbf{r}, \mathbf{r}') + \sin[\theta(\mathbf{r}, \mathbf{r}')]. \quad (1)$$

Here the dots represent time derivatives. The three contributions to $i(\mathbf{r}, \mathbf{r}')$ are the displacement, the dissipative and the superconducting currents, respectively. The phase difference across a junction is $\theta(\mathbf{r}, \mathbf{r}') \equiv \theta(\mathbf{r}) - \theta(\mathbf{r}')$. The currents are expressed in units of the junction critical current I_c ; time is measured in units of the characteristic time $1/\omega_c = \hbar/(2eR_n I_c)$, $\beta_c = (\omega_c/\omega_p)^2$ is the Stewart-McCumber damping parameter [20], with the plasma frequency ω_p defined as $\omega_p^2 = 2eI_c/\hbar C$, and R_n is the junction's normal-state resistance. The RCSJ model has a limitation. It does not take into account that the resistance of a real Josephson junction with high β_c is voltage-dependent: for voltages below the gap voltage the effective resistance is determined by the quasi-particle resistance, which can be orders of magnitude larger than the normal-state resistance [15].

In Fig. 1 we show the geometry of the square array to which most of the results discussed in this paper apply. Each superconducting island is connected to four neighbor islands via identical Josephson junctions. The bias current is fed in at the lower boundary and taken out at the upper boundary.

When we neglect the self-induced magnetic field produced by the current flowing in the array (infinite magnetic penetration depth λ), the array dynamics is described by Eq. (1), together with Kirchhoff's current conservation condition

$$\sum_{\mathbf{a}} i(\mathbf{r}, \mathbf{r} + \mathbf{a}) = i_{\text{ext}}(\mathbf{r}), \quad (2)$$

imposed at every island \mathbf{r} (the summation is over all nearest neighbor islands $\mathbf{r} + \mathbf{a}$). We integrate the coupled equations (1) and (2) using a fast algorithm discussed in [21].

When we include the self-induced fields, thus including screening effects, we redefine $\theta(\mathbf{r}, \mathbf{r}')$ in (1) to be the gauge invariant phase difference across a junction: $\theta(\mathbf{r}, \mathbf{r}') \equiv \theta(\mathbf{r}) - \theta(\mathbf{r}') - 2\pi A(\mathbf{r}, \mathbf{r}')$. The bond frustration variable $A(\mathbf{r}, \mathbf{r}')$ is defined by the line integral of the vector potential \mathbf{A} :

$$A(\mathbf{r}, \mathbf{r}') = \frac{1}{\Phi_0} \int_{\mathbf{r}}^{\mathbf{r}'} \mathbf{A} \cdot d\mathbf{l}, \quad (3)$$

where $\Phi_0 = h/2e$ is the elementary flux quantum. The vector potential is time-dependent, as is the total magnetic flux $\Phi(\mathbf{R}, t)$ at plaquette \mathbf{R} :

$$\frac{\Phi(\mathbf{R}, t)}{\Phi_0} = \sum_{\mathcal{P}(\mathbf{R})} A(\mathbf{r}, \mathbf{r}', t). \quad (4)$$

Here $\mathcal{P}(\mathbf{R})$ denotes an anti-clockwise sum around the plaquette \mathbf{R} . The time-dependent magnetic flux is induced by all the currents flowing in the array via the Faraday-Ampere laws. In zero external magnetic field, we may write

$$\Phi(\mathbf{R}, t) = \sum_{\mathbf{r}, \mathbf{a}} \Gamma(\mathbf{R}, \mathbf{r}, \mathbf{a}) i(\mathbf{r}, \mathbf{r} + \mathbf{a}, t). \quad (5)$$

Γ is a matrix that explicitly depends on the geometry of the array and the junctions. The standard inductance matrix is then given by the discrete curl of Γ . As discussed in more detail in Ref. [22], in the linearized approximation the strength of the self-induced fields is governed by the perpendicular magnetic penetration depth

$$\lambda = \frac{\Phi_0}{2\pi I_c \mu_0}, \quad (6)$$

or equivalently by the κ -parameter

$$\kappa = \frac{\lambda}{a} = \frac{\omega_\Phi}{\omega_c}, \quad (7)$$

where $\omega_\Phi = R_n/(\mu_0 a)$, and μ_0 is the vacuum magnetic permeability. We set the lattice constant a equal to unity and use the parameter λ to indicate the degree of screening.

In our calculations we use the full-range inductance matrix (“Model C” in Ref. [22]). The inductance matrix elements are computed using the model approximations discussed in Ref. [22]. After choosing the temporal gauge, equations (1) to (5) can be combined into one (vector) equation that governs the complete dynamics (see Ref. [22]).

The vorticity $n(\mathbf{R})$ of a plaquette \mathbf{R} is defined as

$$2\pi n(\mathbf{R}) = 2\pi \Phi(\mathbf{R}) + \sum_{\mathcal{P}(\mathbf{R})} (\theta(\mathbf{r}) - \theta(\mathbf{r}') - 2\pi A(\mathbf{r}, \mathbf{r}')). \quad (8)$$

Here the gauge invariant phase difference $\theta(\mathbf{r}) - \theta(\mathbf{r}') - 2\pi A(\mathbf{r}, \mathbf{r}')$ is taken between $-\pi$ and $+\pi$.

We would like to model the vortex motion in the array by a coarse-grained equation of motion as in the Bardeen-Stephen model for flux flow in continuous superconductors. The dissipative currents in the junctions, modeled in Eq. (1) by currents through ohmic shunt resistors, give rise to a viscous force on a moving vortex. Furthermore, in capacitive arrays ($\beta_c > 0$), the electromagnetic energy stored in the junction capacitors due to the vortex motion, can be interpreted as the kinetic energy of a massive vortex [9–14,23]. For an infinite array, and for infinite magnetic penetration depth, a coarse-grained model equation in terms of a single continuous vortex coordinate x reads:

$$M\ddot{x} + \eta\dot{x} = i_b + i_d \sin(2\pi x), \quad (9)$$

where $M = \pi\beta_c$ and $\eta = \pi$ for a square array [9–14,23]. This equation describes the vortex as a point particle with mass M that, driven by a (Lorentz) force proportional to i_b , moves through a sinusoidal pinning potential and experiences a viscous damping force with constant viscosity coefficient η . An estimate for i_d in a square lattice gives $i_d \approx 0.10$ [24]. In a previous paper [5], we have deduced an alternative phenomenological vortex equation of motion with a velocity-dependent vortex viscosity. In contrast to the model with constant viscosity given in Eq. (9), the nonlinear model gives a qualitatively correct account of the numerical results for the current-voltage characteristics calculated using the full set of equations (1). The equation reads

$$M(\beta_c)\ddot{x} + \frac{A(\beta_c)}{1 + B(\beta_c)\dot{x}} \dot{x} = i_b + i_d \sin(2\pi x). \quad (10)$$

Here the phenomenological constants A , B and M are found to be weakly dependent on β_c .

In the model equations (9) or (10) the vortex dynamics is described in terms of a single particle with coordinate x . In writing these equations we assume that, as the vortex moves, it does not couple to other excitations in the array. As a result, it is assumed that the electromagnetic energy associated with the moving vortex, and interpreted as its kinetic energy, can only be absorbed by the viscous medium and not transmitted to other dissipative modes in the array. The limited validity of this assumption is apparent for example from numerical simulations [1,2,4], where no ballistic vortex motion was found when switching off the bias current. Furthermore, it was found in experiments [16] and simulations that the vortex viscosity does not decrease as $1/R_n$ when increasing R_n . The non-zero vortex viscosity in the underdamped limit was understood as due to the coupling of the moving vortex to charge oscillations ('spin waves') [2,7,14,16].

For a finite array, an extra position-dependent force due to the vortex-boundary interaction should enter at the right-hand side of these equations:

$$M\ddot{x} + \eta\dot{x} = i_b + i_d \sin(2\pi x) - F(x), \quad (11)$$

and

$$M(\beta_c)\ddot{x} + \frac{A(\beta_c)}{1 + B(\beta_c)\dot{x}} \dot{x} = i_b + i_d \sin(2\pi x) - F(x). \quad (12)$$

To compute this force, one has to take into account all the infinitely many image vortices that are produced by the array boundaries. When we take the origin at the left-hand side boundary of the array, this leads to the following form of the force:

$$F(x) = -\frac{d}{dx} \ln\left(\frac{2L}{\pi} \sin\left(\frac{\pi x}{L}\right)\right). \quad (13)$$

In order to avoid the singularities at the boundaries in (13), we use a cutoff: for distances to the boundaries smaller than half a lattice constant, we set $F(x) = 0$. Note that this cutoff prescription fixes the maximum attractive force due to the boundary on the vortex at $F_{\max} = F(x = \frac{1}{2})$. In Ref. [13] it is argued that the vortex mass increases close to a free boundary. It was found that this increase is only noticeable within one lattice constant from the boundary. We do not include this quantitative correction in the models (11) and (12), as the arbitrariness of the cutoff prescription already makes that the results are only qualitative in nature.

III. RESULTS

A. $\lambda = \infty$

In Fig. 2 we present a summary of the results for a 16×16 square array with $\lambda = \infty$ for different values of β_c . At the bottom we show the results of the simulations for $\beta_c = 0$, in

which the vortex motion is purely viscous, and the vortex mass is zero. We have considered all current values between $i_b = 0.0$ and $i_b = 1.0$, with a grid of $\Delta i = 0.01$. For this system size the vortex depinning current is between 0.11 and 0.12, so for currents $i_b \leq 0.11$ the vortex is pinned to the middle plaquette of the array, and for $i_b \geq 0.12$ it is depinned (If one increases the system size the depinning current will reach the value $i_d = 0.10$ estimated in Ref. [24] for an infinite array). When the vortex is depinned and moves towards one of the free boundaries, the approach to its image on the other side of the boundary causes it to accelerate. When the vortex reaches the boundary, it leaves the array, or, equivalently, it is annihilated by its image antivortex. We denote this behavior as type **A**.

Above $i_b = 0.96$ the $\beta_c = 0$ dynamics loses its single-vortex character after a short transient time, when additional vortices are generated in other rows. In fact the measured voltage is due to the motion of vortices in all rows. As we want to focus on the single-vortex dynamics in this paper, we will not go further into this type of motion here.

For nonzero β_c , we started the simulations at $t = 0$ increasing the current linearly from zero to i_b in one RC time of the junctions. The relaxational oscillations due to this increase in the current decay while the vortex is moving towards the boundary. We checked that the behavior at the boundary is not seriously affected by these relaxational oscillations by comparing the results to those in a 32×16 array.

For $\beta_c = 2$, the results for the vortex propagation are similar to the $\beta_c = 0$ results. The only difference is that the regime with type **A** behavior now ends at $i = 0.86$ due to the onset of row switching, which means that the vortex switches one or more rows of longitudinal junctions (i.e. junctions in the current direction) into the resistive state [1–3,25].

For $\beta_c \geq 2.5$ a current range opens up in which the vortex is reflected as an antivortex at the boundary in a way a soliton reflects in a long Josephson-junction (LJJ) [17,18]. Alternatively, one may say that the vortex and its antivortex image pass through each other, analogously to the non-destructive soliton-antisoliton collisions in a LJJ [17,19]. The antivortex in turn is reflected at the opposite free boundary as a vortex. This sequence repeats so that the vortex/antivortex never escapes from the array, thus producing a non-zero time-averaged voltage perpendicular to the vortex motion. We denote this as type **B** behavior. In a LJJ a similar type of soliton motion gives rise to the first zero-field step [20]. Although there are important differences between the properties of solitons in a continuous junction and the properties of vortices in the discrete array, it appears, in the regime considered here, that their reflection properties at a boundary as well as their collision properties are similar in many respects. For a two-dimensional array of Josephson junctions the non-destructive collision of a vortex-antivortex pair has been alluded to by Nakajima and Sawada, in the context of a model including the self-inductances of the plaquettes [26].

In Fig. 3 we show the voltage versus current characteristic for $\beta_c = 10$. We note that for the calculation of this current-voltage characteristic we use the same initial phase configuration for all the bias currents considered. Above the vortex depinning current, we start the calculation of the time-averaged voltage only after a sufficiently long time interval for the vortex to reach the boundary. As a result, in the case of type **A** behavior we measure no voltage, as there is no dissipation after the vortex escapes from the array. In contrast, the type **B** regime has a non-zero voltage. The current-voltage characteristic has a considerable slope in this regime, in contrast to the first zero-field step in a LJJ, which is much flatter, due to the fact that the voltage is limited by the maximum soliton velocity. For even higher

currents, we enter the row-switching regime with a large voltage increase.

We interpret the type **B** behavior as being the result of the inertia, or kinetic energy, carried by the vortex. The attractive interaction between the vortex and its image provides a potential well from which the reflected antivortex has to escape after the reflection/collision, in order to travel towards the opposite boundary. The Lorentz force on the antivortex due to the applied bias current is in itself not sufficient to pull it out of the well. In addition, the vortex needs to have a minimum kinetic energy in order to escape: this will be the case if both the vortex mass $M = \pi\beta_c$ as defined in equation (9) and the vortex velocity (monotonically increasing with i_b) are sufficiently large. In Fig. 4 we show snapshots of the vortex configurations at different times for $\beta_c = 10$ and $i_b = 0.49$. In Fig. 5 we show the time-dependent voltage across the array indicating the times at which the snapshots shown in Fig. 4 are taken. The large voltage fluctuations for short times are due to the additive contributions of the relaxational oscillations of all the individual longitudinal junctions in the array as the bias current is changed from zero to 0.49 in the time interval $0 < t < 10$. For $t > 100$ these oscillations have relaxed sufficiently and the vortex contribution to the voltage becomes dominant. As the vortex approaches the boundary its velocity increases and so does the voltage. At the reflection, the vortex velocity jumps from a maximal value (just before the reflection) to a minimal value (just after the reflection).

To verify the interpretation of the vortex reflection as a non-destructive collision with the image antivortex, we have investigated the collision properties of a vortex-antivortex pair explicitly. This entails simulations of a 16×32 square array with *periodic boundary conditions* in the direction of the vortex motion, with one vortex and one antivortex separated by 16 lattice constants present in the initial phase configuration. This situation is the explicit realization of the image-vortex system corresponding to the 16×16 array with free boundaries and a single vortex. Below the row-switching threshold, we find that indeed the corresponding vortex dynamics, i.e. destructive collision **A'** and non-destructive collision **B'**, takes place. The transition between the types **A'** and **B'** behavior is at a current value close to the one between types **A** and **B** in the finite array with one vortex, thus providing a phenomenological explanation of the results.

For currents in the type **A'** regime close to **B'**, the destructive collisions become a two-stage process: first the vortices collide non-destructively, drift three lattice constants apart and then fall back onto each other and annihilate. In the LJJ-soliton language this is called a decaying breather mode. In the finite array the corresponding process in the **A** range (near to the **B** range) consists of a reflected antivortex that falls back over the edge. We interpret this process as evidence for a non-zero vortex mass: the vortex moves up-hill (in the potential landscape) until it reaches a turning point where the kinetic energy is used up, and then falls back in the potential well.

When β_c increases, the lowest current resulting in type **B** behavior decreases, as shown in Fig. 2. The current for row-switching decreases as well, similar to the β_c dependence of the row-switching threshold in previous simulations with periodic boundary conditions [1–3,5]. In the next section we will interpret the type **A** versus type **B** behavior in terms of the coarse-grained model equations given in Eqs. (11) to (13) of a vortex interacting logarithmically with its image(s).

For $\beta_c \geq 50$ we observe the sequence **A** \rightarrow **B** \rightarrow **A** \rightarrow **B** as a function of bias current: the type **B** regime splits up into two pieces separated by a second type **A** regime. The

second type **A** regime is due to the presence of charge oscillations on the shunt capacitors, which become larger in amplitude for increasing β_c . At the reflection, the vortex velocity becomes so large, that additional dissipative modes in the array are excited in the form of local charge oscillations on the shunt capacitors. These oscillations interfere with the motion of the antivortex, which as a result is slowed down and cannot escape from the potential well. For higher currents, there is a second **B** region. Here the antivortex has a higher velocity, and it is able to survive the coupling to the charge fluctuations. The magnitude of the second **A** regime grows with β_c , and we have found that for $\beta_c = 500$ there are no **B** regimes left. We note that the break up of the type **B** regime into two pieces and the disappearance of the reflection for very low damping have no counterpart in the context of a soliton moving in a LJJ.

One might ask if the collision can still be non-destructive if the vortices collide along a direction that is not parallel to one of the coordinate axes. We have simulated a finite 16×16 square array with $\beta_c = 10$ containing a vortex and an antivortex that are inserted not in the same row but in adjacent rows. The results show a reduced but non-vanishing current regime ($0.63 \leq i_b \leq 0.66$) for reflections for both vortices at the edges plus a ‘new’ non-destructive collision in the middle of the array, during which the vortices interchange rows, as shown in Fig. 6.

B. Finite λ regime

Thus far we have studied the reflection properties of the vortex in an array with zero self-induced magnetic fields, or equivalently, with magnetic penetration depth λ much larger than the array size. From the point of view of for example arrays made of niobium junctions, in which the self-induced magnetic fields are non-negligible [27], it is important to see how these fields influence the reflection properties of a vortex. We have therefore studied the vortex propagation in 16×16 square arrays for a range of λ values at $\beta_c = 10$ and 100. We find that the reflection still occurs for finite λ . The results are shown in Figs. 7 and 8. As discussed by Phillips et al. [27], the vortex depinning current is enhanced by the self-induced fields. For example, for our 16×16 array with $\lambda = 0.3$ and $\beta_c = 100$ we find that the vortex depins for currents larger than or equal to $i_b = 0.38$. For $\beta_c = 10$ and in the type-II regime (λ larger than a few lattice spacings) the width and the position of the **B** regime is somewhat insensitive to the λ value as one can see in Fig. 7. As we see in Fig. 8 for $\beta_c = 100$, the second **A** regime shrinks with decreasing λ , and disappears for $\lambda < 5$. For $\lambda \leq 1$ (type-I) we find that the **B** regime shrinks, both for $\beta_c = 10$ and $\beta_c = 100$.

IV. COMPARISON WITH THE PHENOMENOLOGICAL MODEL EQUATIONS

In this section we will make a qualitative comparison of the $\lambda = \infty$ results presented in section III with the results for the vortex motion in a finite array based on Eqs. (11) and (12).

Naively, in Eq. (13) the parameter range for x is $0 \leq x \leq L$. However, when the vortex reflects at $x = L$, the positive image vortex of the reflected antivortex has a coordinate $x > L$, and we can interpret the oscillating state (type **B** behavior) as the motion of a

positive vortex through the force field $F(x)$, periodically extended to the complete real axis. **A** behavior then corresponds to trapping of the vortex around $x = L$ (modulo L). Starting from $x = 8$ at each current value considered, we calculated the current-voltage characteristic numerically from Eqs. (11) and (13) for $L = 15$, using the cutoff prescription mentioned above. The results for $\beta_c = 10$ are shown as the dashed line in Fig. 3. The model underestimates the threshold for type **B** dynamics. As this threshold is very sensitive to the type of cutoff used, we can not draw quantitative conclusions about the vortex mass from this result.

We have determined the threshold currents $i_{A \rightarrow B}$ as a function of β_c from the model equation (11), as well as from the same equation with the nonlinear friction term from Eq. (12). We find that the dependence of the $A \rightarrow B$ threshold current on β_c is qualitatively the same as found in the simulations. In the models the decrease of the threshold value is due to the increase in the mass parameter $M = 2\pi\beta_c$, which increases the vortex kinetic energy. The larger this kinetic energy is, the easier it is for the vortex to escape from the effective potential well.

We note that the way in which vortex inertia manifests itself, and hence the (possible) attribution of a mass, depends on the dynamical situation considered. In previous simulations [1,2,4], in contrast to this work, the vortex mass was probed by switching off the bias current. Changing the current gives rise to enhanced local relaxational oscillations in the junction phases near to the vortex center, or in other words, to a coupling to other dissipative modes in the array. Instead of allowing the vortex to continue its motion, the electromagnetic energy stored in the capacitors then leads to local oscillations. For large β_c these force the vortex center to oscillate back and forth a couple of times between two adjacent plaquettes, as shown for $\beta_c = 2500$ in Fig. 10 of Ref. [2]. During the decay of these oscillations the electromagnetic energy is dissipated. The distance traveled by the vortex after the current has been turned off, is zero. Therefore the mass attributed to the vortex in this situation is zero or very small. Similarly, probing the vortex mass by looking at the hysteresis in the I-V characteristics [3,5], which also involves changes in the current bias, leads to zero or very small phenomenological mass $M(\beta_c)$ in (10) for moderate values of β_c [5].

On the basis of the model interpretation, one would expect that, for some currents just below the transition to type **B** behavior, the reflected antivortex is not falling back over the boundary, but it is re-trapped by the lattice. This re-trapping is then the effect of the combination of the pinning modulation of the effective potential and the energy loss due to friction. We have looked for such a re-trapping process in the simulations for $\beta_c = 100$, and indeed found it for $i_b = 0.2462$ (16×16 array). The reflected antivortex is re-trapped in the second plaquette from the boundary.

V. VORTEX REFLECTION IN DIAGONAL ARRAYS

An important question is how robust the vortex reflection at a boundary (or the non-destructive collision of a vortex-antivortex pair) is for other array geometries. We have studied the case in which the current is injected not along one of the coordinate axes, but along the $-x$ and y direction. See Fig. 9, that shows a 15×15 diagonal array, in which the initial position of the vortex is indicated by an open circle. The vortex will move at

45 degrees to the boundary, due to the diagonal current bias, which allows us to study the reflection behavior for this angle of incidence. We also find soliton-like reflection in this case, albeit the width of the current regime is smaller, and vanishes again already at a β_c value somewhere between 50 and 100. Although the vortex and its image collide at an angle of 90 degrees, the reflecting antivortex still retraces the path of the incident vortex. This is basically because the antivortex has to travel at right angles to the applied bias current. An interesting question would then be what happens for a reflection at zero current bias. To study this within the setting of our model simulation, one would need a nonzero current first to depin the vortex and then switch the current off just before the reflection. However, it is known [1,2,4] that switching off the bias current is not followed by a propagation of the vortex for β_c in the range in which we find vortex reflection. Therefore, switching off the bias current just before the reflection does not seem to be an option to study reflection at zero bias current.

VI. SUMMARY AND DISCUSSION

In conclusion, we have performed RCSJ-model simulations of a finite Josephson-junction array containing a single vortex in a dc current bias. For moderate damping, we find current regimes where the vortex reflects at the boundary, moving back as an antivortex towards the opposite boundary, where the dual reflection process takes place, leading to a stationary oscillatory state and a non-zero time-averaged voltage across the array. This oscillatory motion can be viewed as a discrete analogue of the bouncing of a soliton in an underdamped long Josephson junction, which gives rise to the first zero-field step [17]. The long Josephson junction or Josephson transmission line can be used as a vortex flow transistor or oscillator in many different devices [28]. Recently, Van der Zant and Orlando [29] explored the possibility of using a discrete one-dimensional parallel array of underdamped junctions as a vortex flow transistor. Some time ago it has been shown numerically [30] as well as experimentally [31,32] that vortices in a 1D parallel Josephson array have soliton-like collision properties. Our results show that the soliton-like collision and reflection also occur in two-dimensional arrays, and that the first zero-field step has a discrete analogue in JJA, which suggests a possible use of the two-dimensional array as a vortex-flow device. An important difference found with respect to the soliton motion in LJJ for very low damping, is the fact, that in the array the reflection is absent for values of β_c of the order of 500 and larger [19].

When considering a vortex-antivortex pair in an array with periodic conditions, the vortices collide non-destructively for appropriate bias currents. This is the behavior equivalent to the reflection of one vortex at a free boundary. Our numerical results can be interpreted in terms of a macroscopic model equation for a massive vortex. We also studied the vortex propagation in a diagonal array where the vortex has an angle of incidence of 45 degrees to the boundary, and found that, for appropriate bias currents, reflection takes place here as well. Finally, we also studied the effect of self-induced magnetic fields, using a model that takes into account the full inductance matrix of the array and found that the same type of vortex reflection regimes as in the $\lambda = \infty$ case are present for a range of values of λ and β_c .

ACKNOWLEDGMENTS

We thank J.E. Mooij for suggesting the topic of this work. We also thank him and W. Elion, P. Hadley, A. van Oudenaarden and H. van der Zant for discussions. This work was supported in part by the Dutch organization for fundamental research (FOM). The work of JVJ has been partially supported by NSF grant No. DMR-9521845.

* Present address: Institut für Theoretische Physik, Universität Würzburg, Am Hubland, 97074 Würzburg, Germany.

REFERENCES

- [1] P.A. Bobbert, Phys. Rev. B **45**, 7540 (1992).
- [2] U. Geigenmüller, C.J. Lobb, and C.B. Whan, Phys. Rev. B **47**, 348 (1993).
- [3] W. Yu, K.H. Lee, and D. Stroud, Phys. Rev. B **47**, 5906 (1993).
- [4] W. Yu and D. Stroud, Phys. Rev. B **49**, 6174 (1994).
- [5] T.J. Hagenaars, P.H.E. Tiesinga, J.E. van Himbergen, and J.V. José, Phys. Rev. B **50**, 1143 (1994).
- [6] T.J. Hagenaars, P.H.E. Tiesinga, J.E. van Himbergen, and J.V. José, Quantum Dynamics of Submicron Structures, Vol 291 of NATO Advanced Studies Institute, Series E: Applied Sciences, edited by H.A. Cerdeira *et al* (Kluwer, Dordrecht 1995), p. 617.
- [7] U. Geigenmüller, preprint (1995).
- [8] E. Šimánek, *Inhomogeneous Superconductors*, Oxford University Press, New York 1994.
- [9] A.I. Larkin, Yu. N. Ovchinnikov, and A. Schmid, Physica **152B**, 266 (1988).
- [10] U. Eckern and A. Schmid, Phys. Rev. B **39**, 6441 (1989).
- [11] U. Eckern, in *Applications of Statistical and Field Theory Methods to Condensed Matter*, Vol. 218 of NATO Advanced Studies Institute, Series B: Physics, edited by D. Baeriswyl *et al.* (Plenum, New York 1990), p. 311.
- [12] M.S. Rzchowski, S.P. Benz, M. Tinkham, and C.J. Lobb, Phys. Rev. B **42**, 2041 (1990).
- [13] T.P. Orlando, J.E. Mooij, and H.S.J. van der Zant, Phys. Rev. B **43**, 10218 (1991).
- [14] U. Eckern and E.B. Sonin, Phys. Rev. B **47**, 505 (1993).
- [15] H.S.J. van der Zant, F.C. Fritschy, T.P. Orlando, and J.E. Mooij, Europhys. Lett. **18**, 343 (1992).
- [16] H.S.J. van der Zant, F.C. Fritschy, T.P. Orlando, and J.E. Mooij, Phys. Rev. Lett. **66**, 2531 (1991); Phys. Rev. B **47**, 295 (1993).
- [17] T.A. Fulton and R.C. Dynes, Solid State Comm. **12**, 57 (1973).
- [18] K. Nakajima, Y. Onodera, and Y. Ogawa, J. Appl. Phys. **47**, 1620 (1976).
- [19] D.W. McLaughlin and A.C. Scott, Appl. Phys. Lett. **30**, 545 (1977).
- [20] see for example: K.K. Likharev, *Dynamics of Josephson Junctions and Circuits* (Gordon and Breach, New York, 1986).
- [21] H. Eikmans and J.E. van Himbergen, Phys. Rev. B **41**, 8927 (1990); A similar but even faster algorithm was introduced in D. Domínguez, J.V. José, A. Karma, and C. Wiecko, Phys. Rev. Lett. **67**, 2367 (1991).
- [22] D. Domínguez and J.V. José, Int. J. Mod. Phys. B **8**, 3749 (1994).
- [23] H. Eikmans and J.E. van Himbergen, Phys. Rev. B **45**, 10597 (1992).
- [24] C.J. Lobb, D.W. Abraham, and M. Tinkham, Phys. Rev. B **27**, 150 (1983).
- [25] H.S.J. van der Zant, F.C. Fritschy, T.P. Orlando, and J.E. Mooij, Physica (Amsterdam) **165&166B**, 969 (1990); and H.S.J. van der Zant, C.J. Muller, L.J. Geerligs, C.J.P.M. Harmans, and J.E. Mooij, Phys. Rev. B. **38**, 5154 (1988).
- [26] K. Nakajima and Y. Sawada, J. Appl. Phys. **52**, 5732 (1981).
- [27] J. R. Phillips, H. S. J. van der Zant, J. White, and T. P. Orlando, Phys. Rev. B **47**, 5219 (1993).
- [28] N.F. Pedersen, IEEE Trans. Magn. **27**, 3328 (1991).
- [29] H.S.J. van der Zant and T.P. Orlando, J. Appl. Phys. **76**, 7606 (1994).
- [30] K. Nakajima and Y. Onodera, J. Appl. Phys. **49**, 2958 (1978).
- [31] A. Fujimaki, K. Nakajima, and Y. Sawada, Phys. Rev. Lett. **59**, 2895 (1987).

- [32] K. Nakajima, H. Mizusawa, Y. Sawada, H. Akoh and S. Takada, Phys. Rev. Lett. **65**, 1667 (1990).

FIGURES

FIG. 1. Square array geometry used in the simulations, illustrated with a 8×8 array. Junctions are denoted as crossed bonds. Free boundary conditions are imposed in both directions, while the current bias is applied along the y -direction.

FIG. 2. Results for different values of β_c for a 16×16 square array with free boundaries. The dashed lines represent the current ranges for which type **A** behavior (vortex escapes from array) was found. The thick lines denote the type **B** ranges (trapped vortex oscillating in the array) and the thin full lines the row-switching regimes.

FIG. 3. Current-voltage characteristics for $\beta_c = 10$, from simulations of a 16×16 square array with one vortex (full line). $\langle V \rangle_t$ is the time-averaged voltage across the array in the current direction, in units of $I_c R_n$ and normalized by the number of longitudinal junctions. The dashed line is the I-V characteristic computed from the linear viscosity model (11).

FIG. 4. Snapshots of the vorticity distribution Eq. (8) in a 16×16 square array with $\beta_c = 10$ and $i_b = 0.49$, showing type **B** dynamics. In the frame labeled with 0 the vortex (black square \equiv vortex center plaquette) is moving towards the right free boundary. After reflection it travels as an antivortex (white square) towards the opposite boundary (frames 1 and 2), where it is reflected again as a positive vortex (frame 3). The snapshots correspond to the instants indicated in Fig. 5.

FIG. 5. Voltage, normalized as in Fig. 3, versus time across a 16×16 square array with one vortex, for $\beta_c = 10$ and $i = 0.49$. The times labeled with 0 to 3 correspond to the respective snapshots shown in Fig. 4.

FIG. 6. Snapshots of the vorticity distribution for a 16×16 array with free boundaries and $i_b = 0.65$, with one positive vortex and one antivortex moving in adjacent rows. The notation is as in Fig. 4. Both vortices reflect at the edges (between frames 0 and 1), and collide constructively in the middle of the array (between 2 and 3), interchanging rows.

FIG. 7. Results for different values of λ for a 16×16 square array with free boundaries at $\beta_c = 10$. The notation is the same as in Fig. 2.

FIG. 8. Results for different values of λ for a 16×16 square array with free boundaries at $\beta_c = 100$. The notation is the same as in Fig. 2.

FIG. 9. Diagonal array geometry used in the simulations, illustrated with a 15×15 array. For clarity we omitted the crosses on the bonds. In both directions free boundary conditions are imposed, while the current bias is applied along a diagonal direction. The open circle denotes the initial position of the vortex.

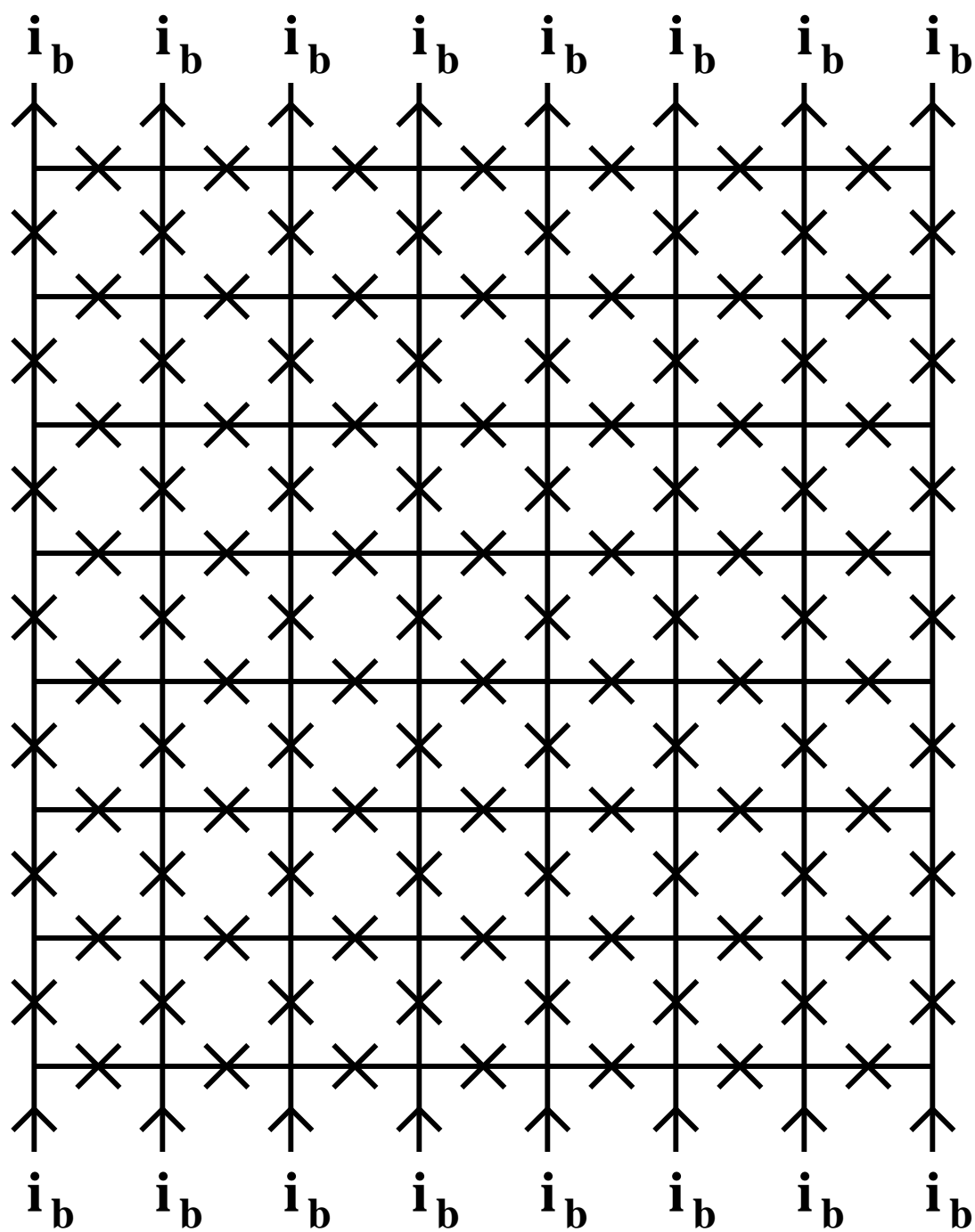


Figure 2

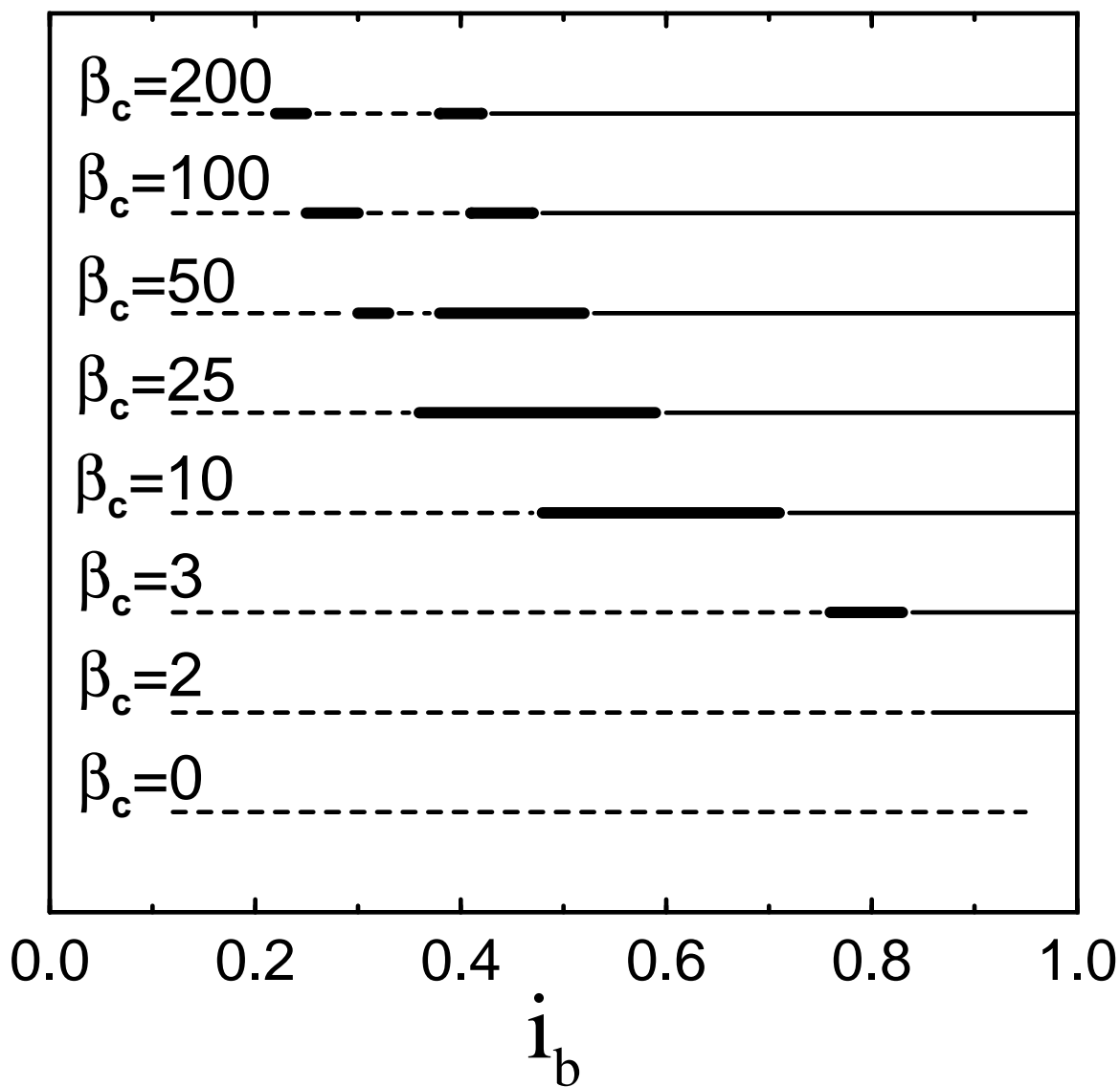
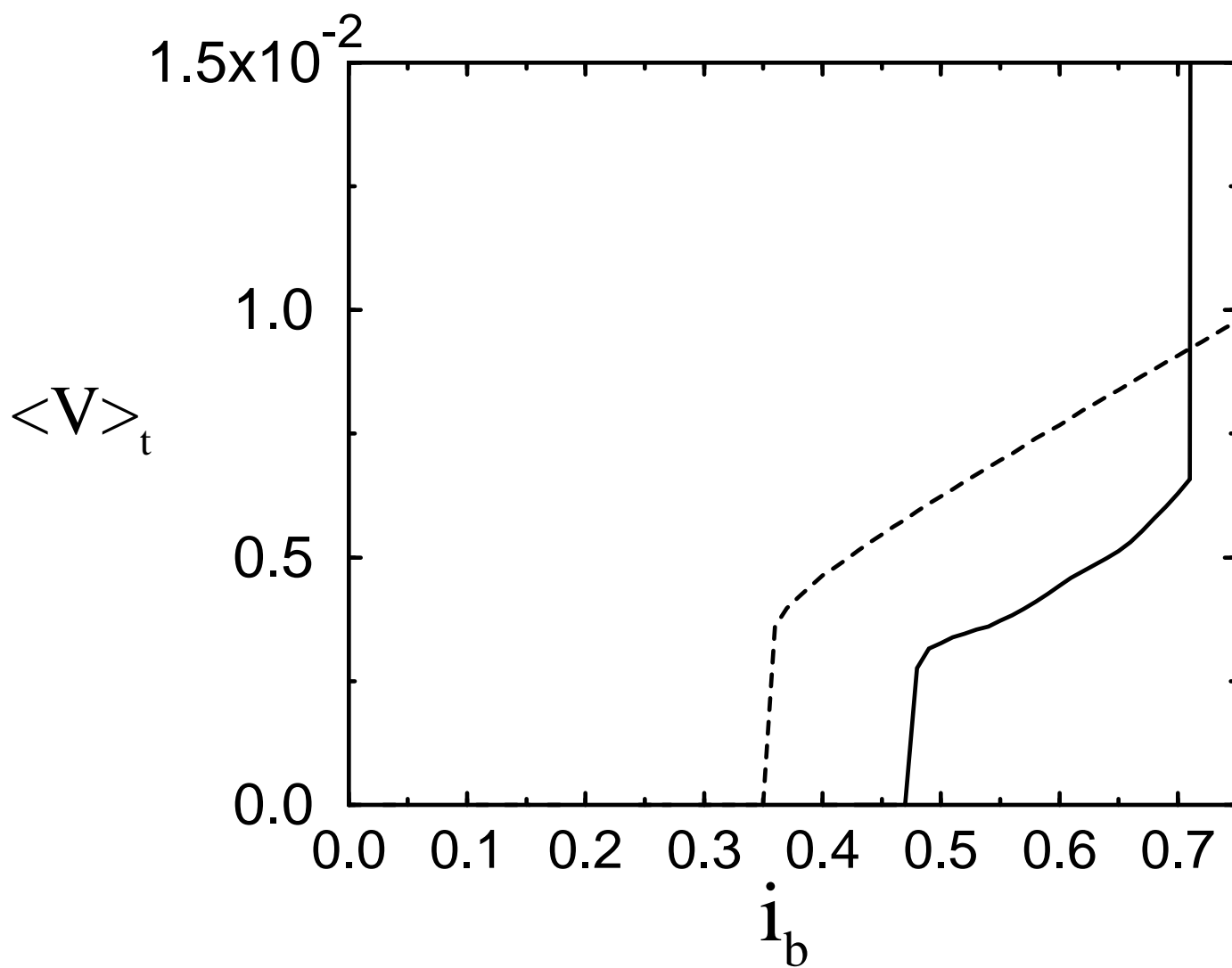


Figure 3







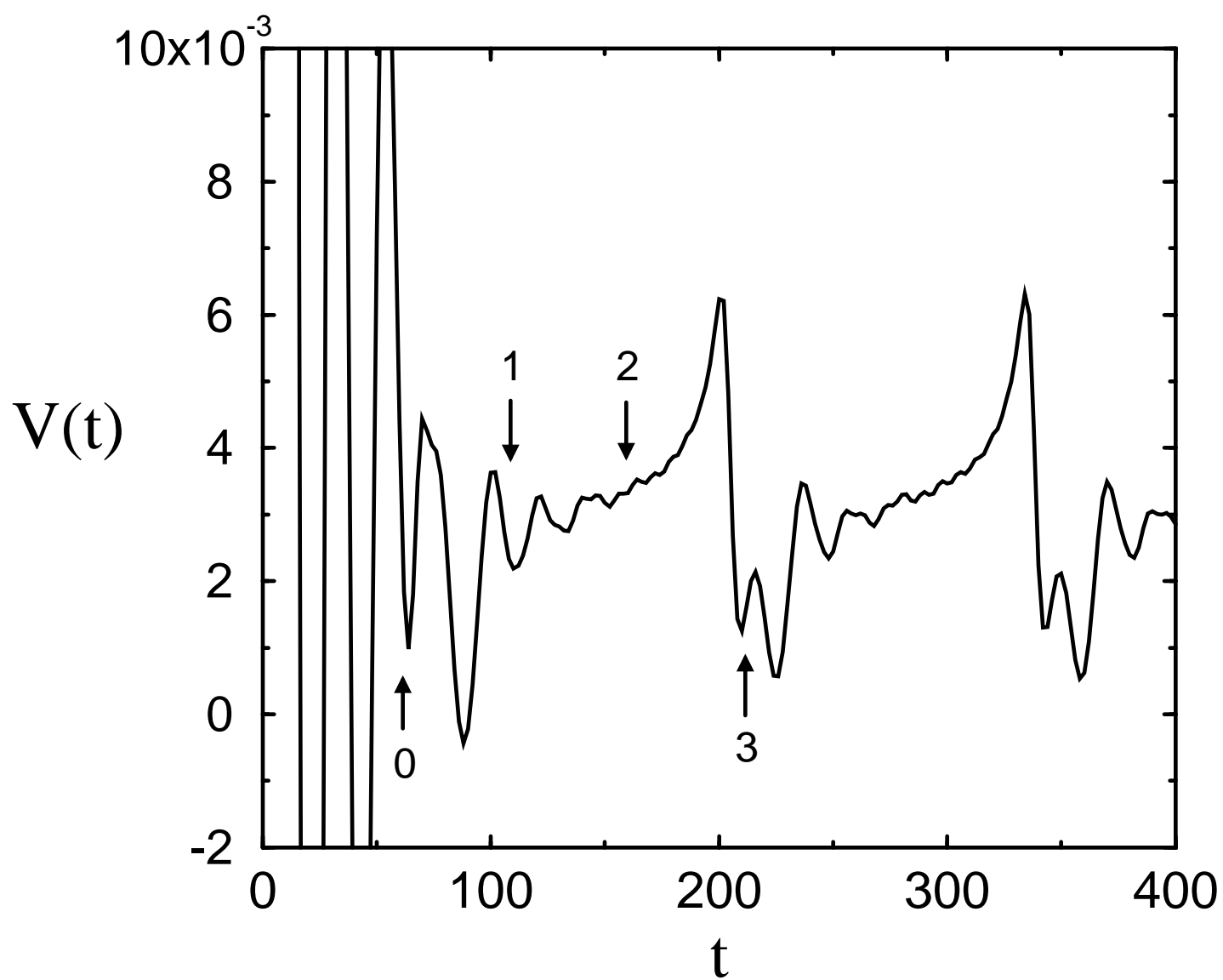
0	
1	
2	
3	

Figure 5



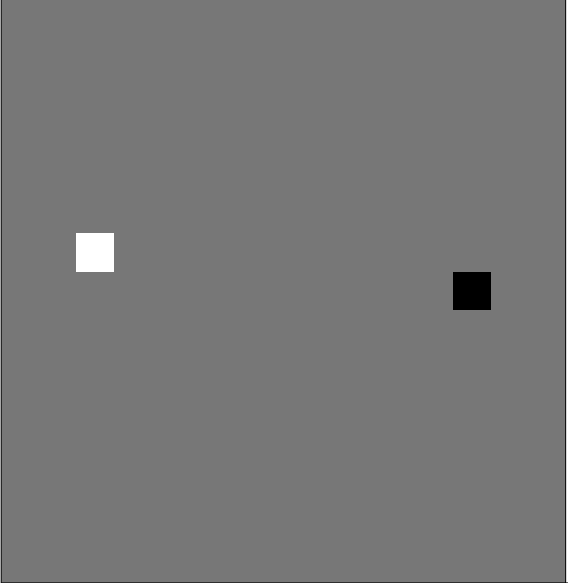
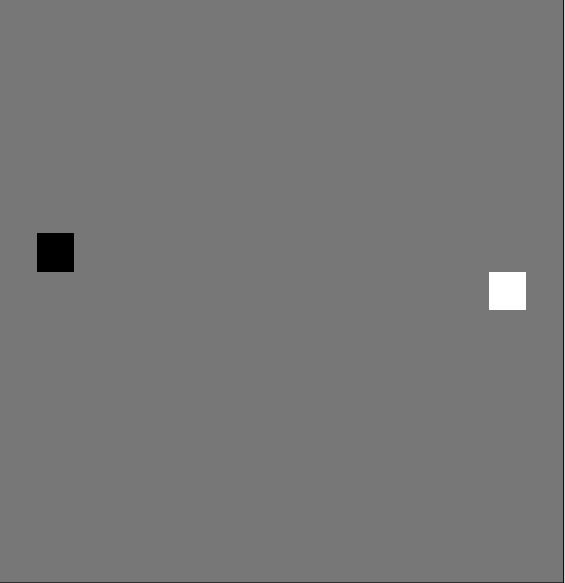
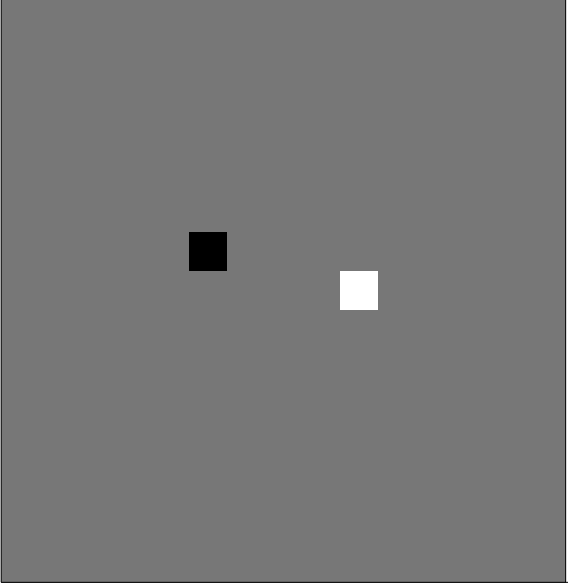
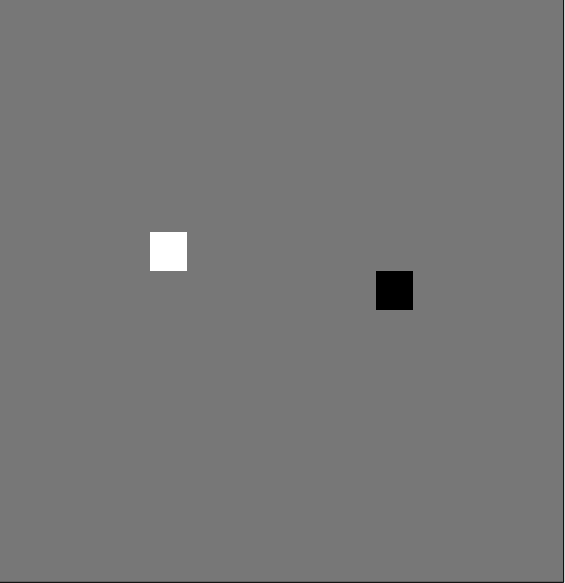
0	1
	
2	3
	

Figure 7

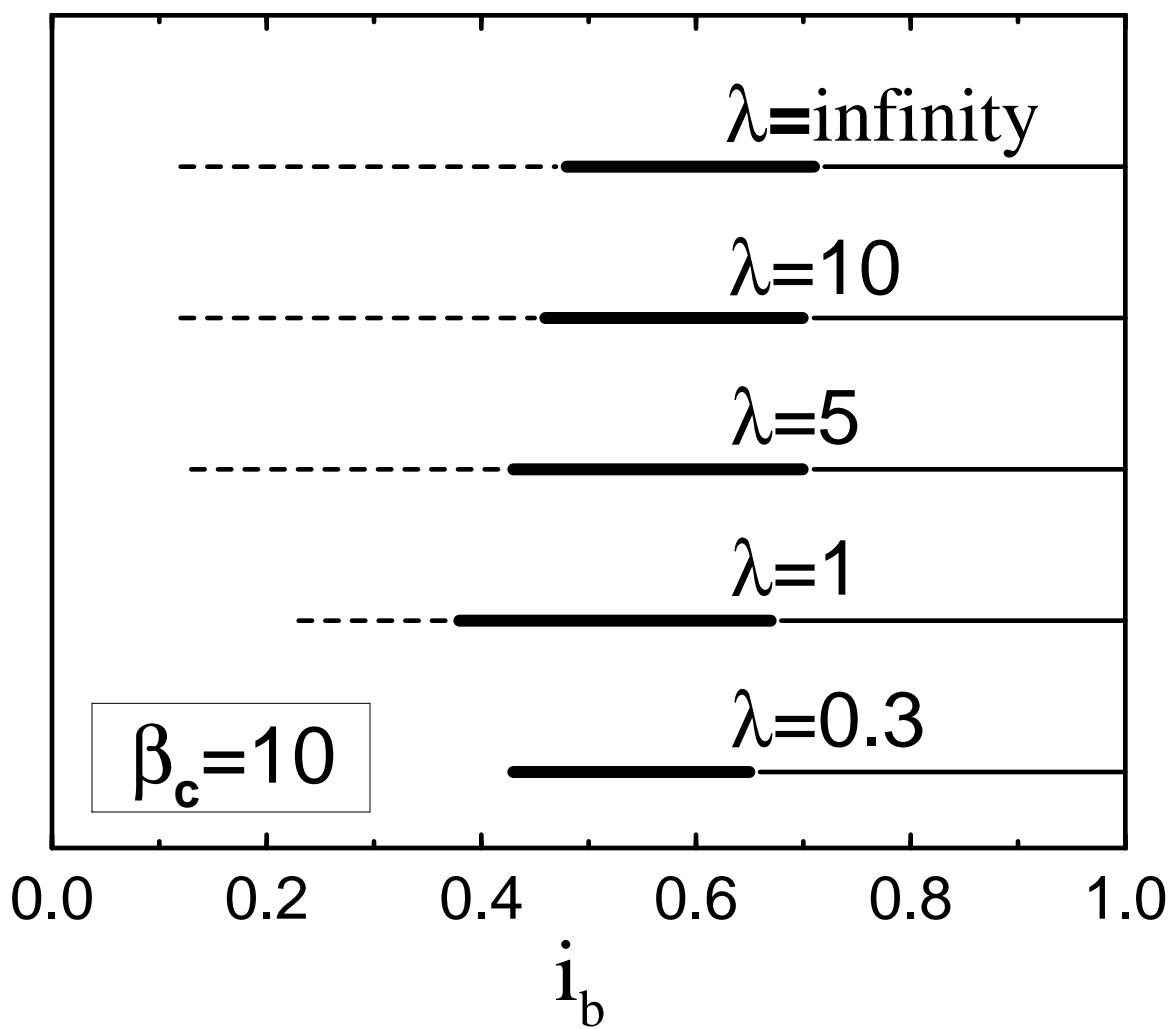


Figure 8

